ELSEVIER

Chemical Geology 227 (2006) 154–164

CHEMICAL GEOLOGY
INCLUDING
ISOTOPE GEOSCIENCE

www.elsevier.com/locate/chemgeo

Thermodynamic modelling of aqueous CH_4-bearing fluid inclusions trapped in hydrocarbon-rich environments

Régis Thiéry

UMR 6524 'Magmas et Volcans', Université Blaise Pascal, 5, rue Kessler, F-63038 Clermont-Ferrand Cedex, France

Received 14 January 2004; accepted 29 September 2005

Abstract

This paper investigates the microthermometric properties of aqueous CH_4-bearing fluid inclusions entrapped in presence of petroleum. The Daridon equation of state [Daridon, J.L., Lagourette, H., Saint-Guirons, H., Xans, P., 1993. A cubic equation of state model for phase equilibrium calculation of alkane + carbon dioxide + water using a group contribution k_{ij}. Fluid Phase Equilib. 91, 31–54] is used to describe the phase equilibria in the H_2O–CH_4–hydrocarbons systems between aqueous solutions and hydrocarbon phases. Modelling shows that methane solubilities in water vary in a more complex way and at lower levels than predicted by models for H_2O–CH_4–salts systems. Thus, trapping pressures of these fluid inclusions, determined from measurements of CH_4 molalities by Raman spectroscopy [Dubessy, J., Buschaert, S., Lamb, W., Pironon, J., Thiéry, R., 2001. Methane-bearing aqueous fluid inclusions: Raman analysis, thermodynamic modeling and application to petroleum basins. Chem. Geol. 173, 193–205], may be strongly underestimated. The study suggests also that the trapping temperature may be slightly higher than the homogenisation temperature.

Keywords: Fluid inclusions; Equations of state; Water; Petroleum; Liquid–gas immiscibility; Thermodynamics

1. Introduction

In the usual P–T range of sedimentary basins (T between 0 °C and 300 °C, and P below 1 kbar), basinal fluids, mainly composed of water, hydrocarbons and salts, are immiscible (excepted in the case of undersaturated water or petroleum) and separate into one aqueous solution (W) and one hydrocarbon-rich phase (L). During cementation, these fluids, which are in chemical equilibrium, may be trapped in coeval aqueous and petroleum fluid inclusions (heterogeneous trapping).

Microthermometry and spectrometric methods (Raman, etc.) coupled with thermodynamic modelling allow to quantify the characteristics of these fluid inclusions (composition and bulk density) and to estimate the trapping conditions (P_{trap}–T_{trap}) of these fluids (Roedder, 1984; Goldstein and Reynolds, 1994; Diamond, 2002). Such information is particularly valuable for the history reconstitution of sedimentary basins, which can contain substantial amounts of petroleum (Hanor, 1980).

The trapping temperature (T_{trap}) is given by homogenisation temperatures ($T_h^{aq.}$) of an assemblage of aqueous inclusions. The trapping pressure P_{trap} can be obtained by calculating the internal pressure at $T_h^{aq.}$ either (1) in petroleum inclusions or (2) in aqueous inclusions.

The first method requires to calculate the phase diagram of the associated petroleum inclusions (including

E-mail address: r.thiery@opgc.univ-bpclermont.fr.

0009-2541/$ - see front matter © 2005 Elsevier B.V. All rights reserved.
doi:10.1016/j.chemgeo.2005.09.013

gas–liquid immiscibility field and isochores). However, the physico-chemical characterisation of petroleum inclusions is difficult and unsure. Some of the available characterization methods are based on a measure of the gas bubble filling degree at ambient temperature (Aplin et al., 1999; Thiéry et al., 2002) by confocal scanning laser microscopy (Pironon et al., 1998) or by simple visual estimation as used in recent publications by Chen et al. (2003) and Benchilla et al. (2003). However, the determination of the phase diagram and P–T isochore remains still speculative (Thiéry et al., 2002) for petroleum inclusions. In fact, it is not unusual to rely rather on the P_{trap} values estimated from other barometric techniques or by assuming the past geothermal gradient to constrain the modelling of internal P–T conditions of petroleum inclusions.

The second technique, based on the pressure calculation in aqueous inclusions at $T_h^{aq.}$, is easier. However, the state of the art is not always applied for determining P_h^{aq}. It is not rare to see in the recent literature the application of the method of so-called "crossing isochors" (Liu et al., 2003; Benchilla et al., 2003), where the starting point of the isochor of the aqueous inclusion is on the saturation curve of pure water. This procedure is clearly erroneous in the case of coeval fluid inclusions, leading to potential overestimations of trapping temperatures and pressures. Water equilibrates necessarily with petroleum, and as such, it contains some salts and some dissolved hydrocarbons (CH_4, C_2H_6, etc.). Even if these hydrocarbons are often not detectable (Dubessy et al., 2001), they are present and they modify the physico-chemical properties of water. The correct procedure for estimating $P_h^{aq.}$ is given in Dubessy et al. (2001) and Guillaume et al. (2003).

This method requires to know (1) the CH_4 molality measured by Raman spectrometry, at or slightly above the homogenisation point, (2) the NaCl molality estimated by classical microthermometry (Roedder, 1984; Goldstein and Reynolds, 1994), and (3) of course, the $T_h^{aq.}$ homogenisation temperature. The thermodynamic solubility model of Duan et al. (1992) can then be used to estimate $P_h^{aq.}$ from these ($T_h^{aq.}$, CH_4 and NaCl molalities) data. Applications of this technique can be found in Tseng and Pottorf (2002) and in Teinturier et al. (2002).

One aspect, which has never been addressed in the application of this method, is the potential influence of hydrocarbons (C_2H_6, C_3H_8, etc.), which are dissolved in small quantities in water. When they are detected by Raman spectroscopy, these compounds are only present as traces (Chen et al., 2003) in water because of their low solubility. In other cases, small hydrocarbon droplets are clearly visible in aqueous inclusions (Guilhaumou et al., 2000; Dutkiewicz et al., 2003). These observations are evidences that interstitial waters were in equilibrium with a hydrocarbon phase, and a rigorous thermodynamic modelling of these aqueous inclusions requires to consider the complete H_2O–CH_4–hydrocarbons–salts system.

The Duan's model (Duan et al., 1992) is not appropriate for calculating the CH_4 solubility of waters in equilibrium with petroleum. Thus, another thermodymic model, the Daridon equation of state (Daridon, 1992; Daridon et al., 1993), has been selected and is presented first. In a second part, methane solubilities and phase diagrams are calculated for two simple ternary systems (H_2O–CH_4–C_2H_6 and H_2O–CH_4–n-C_4H_{10}) and one complex hydrocarbons mixture. The third and last part gives a method to evaluate the influence of hydrocarbons on the estimations of trapping pressures (P_{trap}). Note that this study does not take into account the influence of salts, as the Daridon equation of state does not include salts.

2. The Daridon equation of state

The Daridon equation of state (Daridon, 1992; Daridon et al., 1993) has been designed to describe the phase equilibria (liquid–gas and liquid–liquid–gas) of mixtures of water, carbon dioxide and paraffins. It is a modified Peng–Robinson equation of state (Peng and Robinson, 1976). It uses two sets of binary interaction parameters: the first one for describing molecular interactions between hydrocarbon and water in the hydrocarbon-rich phase ($k^{H}_{i-H_2O}$), and the second one for describing these interactions, but in an aqueous environment ($k^{W}_{i-H_2O}$). Daridon proposes to write:

- for the hydrocarbon-rich phase,
  $k^{H}_{i-H_2O} = \alpha$,
- and for the aqueous phase
  $k^{W}_{i-H_2O} = \alpha + \beta(T_r)$,
  where α is a constant depending on the type of hydrocarbon, and β is a function depending on the temperature:
  $\beta = \beta_0 + \beta_1 T_r + \beta_2 T_r^2$,
  where β_0, β_1 and β_2 are also constant parameters specific to the i hydrocarbon, and:
  $$T_r = \frac{T}{T_{c,H_2O}},$$
  with T_{c,H_2O} which is the critical temperature of water.

An interpolation function, noted F, ensures the continuity between $k^{H}_{i-H_2O}$ and $k^{W}_{i-H_2O}$:

$$k_{i-H_2O} = (1-F)k^{H}_{i-H_2O} + F\ k^{W}_{i-H_2O}.$$

F is equal to 1 for a water-rich phase and to 0 for a hydrocarbon-rich phase. F depends on x_{H_2O} and x_i:

$$F = \exp\left(-10^{\gamma}\left(\frac{x_i}{x_{H_2O}+x_i}\right)^4\right)$$

where γ is an additional constant parameter.

Values of α, β_0, β_1, β_2 and are γ given in Table 1 for CO_2 and most light hydrocarbons (methane to butane). For heavier hydrocarbons, k_{i-H_2O} are calculated by a group contribution method:

$$\alpha = 0.25n_{CH_3} - 0.00834n_{CH_2},$$

$$\beta_0 = -0.6942n_{CH_3} + 0.03113n_{CH_2},$$

$$\beta_1 = 0.9552n_{CH_3} - 0.1482n_{CH_2},$$

$$\beta_2 = -0.3736n_{CH_3} + 0.0880n_{CH_2},$$

$$\gamma = 0.5n_{CH_3} + 0.5n_{CH_2}$$

where n_{CH_3} and n_{CH_2} are the number of $-CH_3$ and $-CH_2-$ molecular groups in the hydrocarbon molecule. Other binary interaction parameters $k_{i,j}$ between hydrocarbon compounds have been left to 0.

Preliminary calculations have confirmed that the Daridon equation of state describes satisfactorily mutual solubilities of light volatile hydrocarbons (CH_4, C_2H_6, C_3H_8, etc.) in the aqueous phase and of H_2O in the hydrocarbon phase. It describes well the P–T relations of liquid–gas and liquid–liquid–gas phase equilibria. Other studies (Søreide and Whitson, 1992; de Hemptinne et al., 2001; Pedersen et al., 2001; Nasrifar and Moshfegian, 2002; Sørensen et al., 2002) have validated the use of other similar versions of modified Peng–Robinson equations of state (Peng and Robinson, 1976) for predicting mutual solubilities of hydrocarbons and water.

Table 1
Parameters of the Daridon equation of state for calculating the binary interaction parameters between water and light hydrocarbons

Component	α	β_0	β_1	β_2	γ
CH_4	0.50	−1.7885	2.6160	−1.0792	1.0
C_2H_6	0.50	−1.3332	1.7226	−0.5821	1.0
C_3H_8	0.52	−1.4360	1.9280	−0.8210	1.0
C_4H_{10}	0.54	−1.313	1.3750	−0.4012	1.0
CO_2	0.19	−0.6689	0.99967	−0.41224	1.0

3. CH_4 solubilities in H_2O–hydrocarbons systems

Iso-CH_4 solubility curves have been investigated first in two simple ternary mixtures, the H_2O–CH_4–C_2H_6 and the H_2O–CH_4–n-C_4H_{10} systems in order to understand the influence of dissolved hydrocarbons. The phase diagram of a complex H_2O-hydrocarbons mixture simulating the behaviour of petroleum with water is calculated next. Phase diagrams are obtained by using algorithms of Asselineau et al. (1979).

3.1. The H_2O–CH_4–C_2H_6 system

Fig. 1 displays iso-CH_4 solubility curves for the immiscibility field of the H_2O–CH_4–C_2H_6 system calculated with a CH_4 molality of 0.1 molal and increasing C_2H_6 molalities (respectively: 0, 0.05 and 0.1 molal). It shows that equilibrium with a CH_4–C_2H_6 gas mixture extends the immiscibility field at higher pressures than obtained from pure CH_4. For example, an aqueous solution containing dissolved CH_4 at a molality of 0.1 molal and C_2H_6 at a molality of 0.01 molal homogenises at 155 bar instead of 140 bar for a CH_4-bearing only solution with the same CH_4 molality of 0.1 molal (i.e. a relative augmentation of 10% in pressure). If the same Raman spectra detection level holds for C_2H_6 as for CH_4 (0.01 molal, Dubessy et al., 2001), it means that trapping pressures may be underestimated even when no C_2H_6 concentration is detected in the aqueous phase (however, C_2H_6 should be detected by Raman spectroscopy in the gas phase).

3.2. The H_2O–CH_4–n-C_4H_{10} system

Fig. 2A displays iso-CH_4 solubility curves in the H_2O–CH_4–n-C_4H_{10} system, which are calculated for a constant CH_4–n-C_4H_{10} molality ratio of 10:1. Such fluid composition is never found in nature. However, to a first approximation, n-C_4H_{10} grouped with other light volatile hydrocarbons of similar properties can represent such a significative part of the hydrocarbons dissolved in water.

The interest of this diagram is to show the behaviour transition between H_2O–CH_4–C_2H_6 systems to systems containing heavier hydrocarbons. Indeed, one important element of this diagram is the curve, noted as *WLG* (thick black line in Fig. 2A), which marks the occurrence of a triphasic liquid–liquid–gas association. The first liquid is the aqueous phase (W), characterized here by a constant $m_{CH_4}/m_{C_4H_{10}}$ ratio of 10, whereas the second one is a liquid (L) rich in hydrocarbons. The curve ends at a critical liquid–gas point around 140 °C,

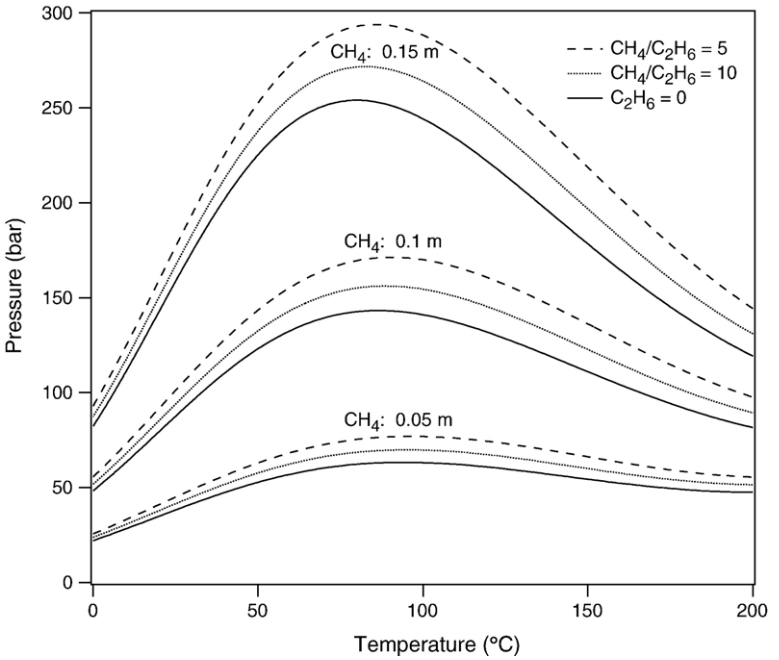

Fig. 1. Iso-CH_4 solubility curves in the H_2O–CH_4–C_2H_6 system calculated with the Daridon equation of state for different ratios of CH_4 and C_2H_6 molalities. Solid lines are curves for the binary system H_2O–CH_4. Numbers indicate CH_4 molalities.

where the n-C_4H_{10}-rich liquid gets similar to the CH_4-rich gas. Below 140 °C, the *WLG* curve splits the phase diagram into two parts: a low-pressure part, where the aqueous phase (*W*) coexists with a CH_4-rich gas (*G*); and a high-pressure part, where the aqueous phase (W) equilibrates with a liquid (*L*) richer in n-C_4H_{10}.

The (*P*–*T*) trends of iso-CH_4 solubility curves change drastically above and below the *WLG* curve and its extrapolation in the supercritical domain in the right part of the diagram (Fig. 2A).

- Below the *WLG* curve, isopleths, noted as *W*(*G*), follow a trend similar to isopleths of the H_2O–CH_4 (Dubessy et al., 2001) or H_2O–CH_4–C2H_6 systems with a bell-shaped morphology (Fig. 1). In this field, the CH_4 solubility is nearly temperature independent. This feature is particularly interesting for barometric estimations (Dubessy et al., 2001).
- To the contrary, above the *WLG* curve, isopleths, noted as *W*(*L*), are much more vertical. In this high-pressure region, the CH_4 solubility is nearly pressure independent. This feature shows clearly that CH_4 molalities cannot be used here as pressure indicators.

The CH_4 solubility varies also in a more complex way. Between 0 and 30 °C, it decreases until a solubility minimum (m_{CH_4}=0.03 m), then increases again with increasing temperatures. However, these CH_4 molalities variations are less than 0.01 molal in this part (T<60 °C) and thus, are below detection level of Raman spectrometry: CH_4 molalities can be considered as nearly constant in this field. Another important remark is the dramatic decrease of CH_4 solubilities as compared to the H_2O–CH_4 system: m_{CH_4} can be divided by a factor up to 2 or 3 (see Fig. 2A, at 100 bar and below 100 °C), when compared to the H_2O–CH_4 system. To the contrary, at temperatures above 60 °C, the CH_4 solubility increases exponentially with the temperature (0.05 molal at 80 °C, 0.1 molal at 140 °C, 0.15 molal at 160 °C, 0.2 at 175 °C, 0.25 molal at 185 °C).

The H_2O–CH_4–n-C_4H_{10} immiscibility fields calculated for other $m_{CH_4}/m_{C_4H_{10}}$ ratios exhibit the same features as described above, i.e. development of liquid–liquid–gas phase equilibria and drastic lowering of dissolved CH_4 in water, when it is in equilibrium with a hydrocarbon fluid of high density.

The consequences of these features must be considered for fluid inclusions studies. Isochoric paths of two fluid inclusions (A and B) are given as example in Fig. 2A (dashed lines) and have been calculated using methods given in Thiéry et al. (2002). Inclusion *A* traps an aqueous solution of m_{CH_4}=0.5 molal and $m_{C_4H_{10}}$=0.05 molal at T=174 °C and P=300 bar, whereas inclusion *B* traps an aqueous solution of m_{CH_4}=0.2 molal and $m_{C_4H_{10}}$=0.02 molal at T=84 °C and P=294 bar. The bulk CH_4–n-C_4H_{10} ratio of these

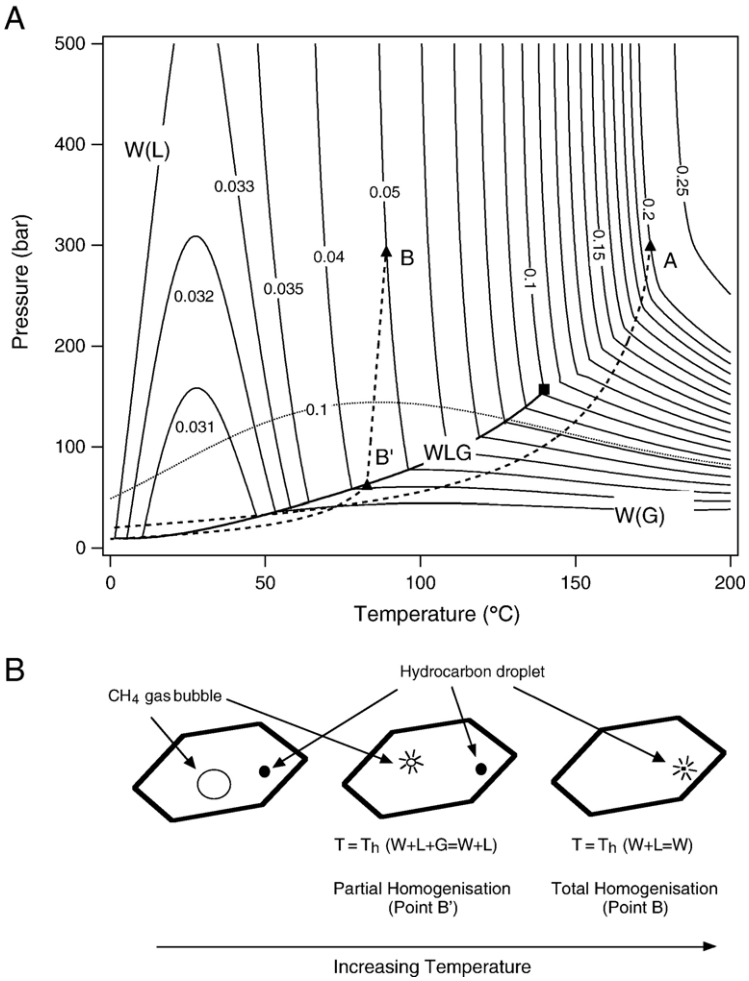

Fig. 2. (A) Iso-CH_4 solubility curves in the H_2O–CH_4–n-C_4H_{10} system calculated with the Daridon equation of state for a constant CH_4/n-C_4H_{10} molality ratio of 10:1. Numbers indicate CH_4 molalities. The thick solid line (WLG) is the locus of liquid–liquid–gas phase equilibria and ends at gas–liquid critical point (filled square). The dotted line is an iso-m_{CH_4} curve in the binary H_2O–CH_4 system (m_{CH_4}=0.1 molal). The dashed curves are P–T isochors of fluid inclusions trapped at A or B points. Numbers indicate CH_4 molalities. (B) Cartoon illustrating the successive phase transitions ($W+G+L \rightarrow W+L$) and ($W+L \rightarrow W$) observed when heating aqueous inclusions equilibrated with a liquid hydrocarbon.

inclusions is 10:1, thus the diagram of Fig. 2 applies to both inclusions.

Inclusion *A* shows the characteristic behaviour of aqueous inclusions containing only volatile components (H_2O–CH_4 or H_2O–CH_4–C_2H_6 systems). This inclusion could be taken as an only CH_4-bearing aqueous inclusion. However, this oversimplification would lead to an underestimation of the trapping pressure by around 98 bar.

Inclusion *B* exhibits a more complex behaviour. The most important fact is that the first phase to form below the trapping point of the inclusion, is not a gas bubble, but a n-C_4H_{10}-bearing droplet (Fig. 2B). Calculations show that this droplet is very small (its filling degree is below 0.01%): thus, it cannot be observed. The gas bubble appears only below 81 °C, and calculations reveal also that it is composed mainly of CH_4. This example is very instructive, and if such similar behaviour occurs in nature, this has important implications for the analysis of microthermometric data of aqueous inclusions.

- Contrary to what was always asserted in the case of the hetereogeneous trapping of aqueous and petroleum inclusions (Dubessy et al., 2001), the homogenisation temperature ($T_h^{aq.}$) of aqueous inclusions may be slightly lower than the trapping temperature by a few degrees. This occurs because interstitial waters were in equilibrium with a hydrocarbon-rich liquid, and not a gas, before entrapment.
- The liquid droplet concentrates also heavier and less volatile hydrocarbons. Contrary to inclusion *A*, analysis of the gas bubble by Raman spectroscopy will probably not detect these hydrocarbons. Thus, it is

possible that such inclusions cannot be distinguished from true aqueous inclusions containing only CH_4. Therefore, in such cases, the trapping pressure cannot be estimated from CH_4 molality in water. For inclusion *B*, the resulting discrepancy is higher than 250 bar for the trapping pressure.

The isochoric path of inclusion B (Fig. 2A) is composed of two parts:

- between points *B* and *B′* (Fig. 2A), the pressure decreases linearly and abruptly. The CH_4-bearing aqueous solution is in equilibrium with an invisible hydrocarbon phase (Fig. 2B).
- at point *B′*, the isochor exhibits a distinct slope break. At lower temperatures, the internal pressure decreases more smoothly. The fluid inclusion contains now a three-phase assemblage *WLG*. Along this isochor portion, the hydrocarbon-rich liquid can be considered as thermodynamically isolated from the aqueous CH_4-bearing part of the system. Thus, the fluid inclusion can be modelled here, to a good approximation, in the H_2O–CH_4 system.

Note also, for a good understanding of Fig. 2A, that the water/*n*-butane ratios of the aqueous phase in inclusions *A* and *B* vary with the temperature and do not keep a constant value of 10:1. As such, no conclusion can be drawn from the relative positions of the isochors with the *WLG* curve, which has been drawn for a constant methane/*n*-butane ratio of 10:1. In this figure, the low-temperature part of the isochor may run above or below this *WLG* curve. In fact, the *WLG* phase association of the water–CH_4–C_2H_6 systems has a variance of 2, as stated by the Gibb's phase rule. Thus, the whole *WLG* field is represented by a surface (not drawn in Fig. 2A) on a *P*–*T* phase diagram.

3.3. A complex H_2O–hydrocarbons mixture

A complex H_2O–hydrocarbons mixture is considered here to model the properties of a water equilibrated with a petroleum. The petroleum composition is given by a specific compositional model for petroleums (the α–β model, see Montel, 1993; Thiéry et al., 2002). α and β are two composition parameters. The following values, $\alpha = 0.94$ and $\beta = 0.514$ used here, are representative of a black oil. Fourteen components, ranging from CH_4 up to n-$C_{16}H_{34}$ are considered in this fluid model. The liquid–gas (LG) immiscibility field of this hydrocarbon mixture is drawn in Fig. 3 and has been calculated with a

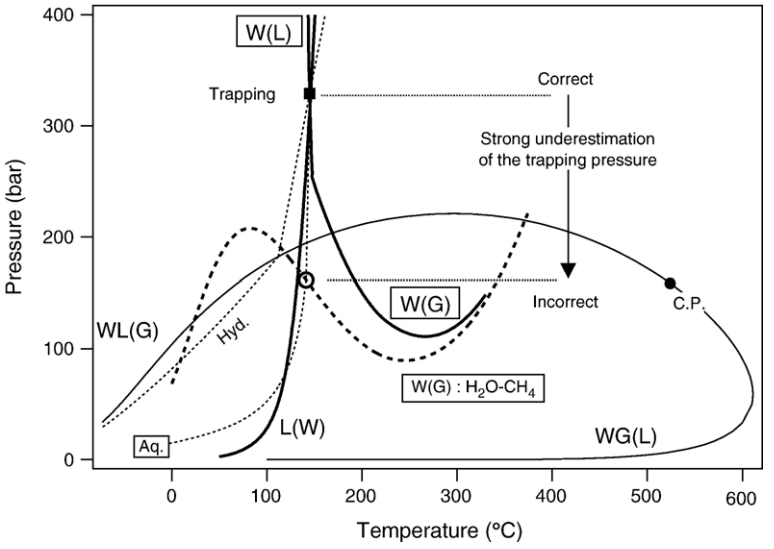

Fig. 3. Superposed theoretical *P*–*T* phase diagrams of coeval petroleum and aqueous fluid inclusions. Elements of the phase diagram of aqueous inclusions are written in framed boxes. The trapping point (T_{trap}, P_{trap}, filled square) is at the intersection of the bubble point curve ($L+W \rightarrow W$) of aqueous inclusions (noted $W(L)$, thick solid line) with the total homogenisation curve ($L+W \rightarrow L$) of petroleum inclusions (noted $L(W)$, thick solid line). The $W(L)$ curve extends at lower pressures to a $W(G)$ curve. The thin solid line delimits the liquid–gas immiscibility field of petroleum inclusions. It has two branches: the bubble point $L(G)$ curve and the dew point $G(L)$ curve which meet at the critical point (C.P., filled circle). Isochors of petroleum inclusions (hyd.) and aqueous inclusions (aq.) are represented by thin dotted curves. The thick dashed curve is the iso-CH_4 solubility curve drawn from the m_{CH_4} measured by Raman spectrometry and calculated by the Daridon equation of state in the H_2O–CH_4 system. The intersection (empty circle) of this curve with the isochor of aqueous inclusions yields the liquid–gas homogenisation of aqueous inclusions. The trapping pressure is strongly underestimated if dissolved hydrocarbons are not considered by thermodynamic modelling.

Peng–Robinson equation of state (Peng and Robinson, 1976) using parameters given in Thiéry et al. (2002). In this example, the trapping conditions have been chosen at T_{trap}=145 °C and P_{trap}=329 bar. The composition of the water equilibrated with this petroleum has been calculated at the indicated T_{trap} and P_{trap} with the Daridon equation of state (Daridon, 1992; Daridon et al., 1993). A value of m_{CH_4}=0.1308 molal has been obtained. Other hydrocarbons compounds are present at much lower levels, ranging from 0.01 molal for C_2H_6 to less than 0.0005 molal for the C_{12+} hydrocarbon fraction. Total homogenisation curves, also calculated by the Daridon equation of state, have been drawn in Fig. 3 and intersect at the trapping point. These are:

1. The total homogenisation curve of aqueous inclusions, along which a biphasic association of water (W) and oil-bearing phase (L) homogenises into a single aqueous phase (W): $L+W \rightarrow W$. This curve will be noted as $W(L)$ and corresponds to a bubble point curve. This is an isopleth, as the water composition is hold constant and is given by the composition calculated at the trapping point. Like inclusion B, this curve is nearly temperature independent. At lower pressures, the curve transforms into a $W(G)$ curve, which means that the water is in equilibrium with a gas. This is marked by a change of the curve morphology, getting similar to $W(G)$ curves of the H_2O–CH_4 system (Fig. 3).
2. The total homogenisation curve of petroleum inclusions, along which the association of hydrocarbon phase (L) and water (W) homogenises into a single hydrocarbon phase: $L+W \rightarrow L$. This curve will be referred to as the $L(W)$ curve. This is a dew curve.

The isochoric paths of petroleum inclusions (Fig. 3) in the biphasic (LG) field are easily obtained with algorithms of Asselineau et al. (1979) and Thiéry et al. (2002). However, isochors of aqueous inclusions are much more difficult to calculate. First, as the trapping point is located on a $W(L)$ curve, the first phase to nucleate by cooling below T_{trap} is a liquid-rich-hydrocarbon. As seen in the previous section, the gas bubble forms at a few degrees below the trapping temperature. Present algorithms (Asselineau et al., 1979; Thiéry et al., 2002), which are only able to calculate isochors in monophasic or biphasic fields, are not adequate here, as three phases are involved below T_h^{aq}. Moreover, calculations are made more complex because of the large number of components and the presence of heavy hydrocarbons. Thus, to simplify the problem, it is assumed that at temperatures below $T_h^{aq.}$, the isochor can be calculated by assimilating the fluid inclusion to a H_2O–CH_4 system only. This hypothesis is probably justified, as the hydrocarbon-rich liquid is very small and does not interact chemically with the aqueous and gaseous parts of the inclusion for temperatures below T_h^{aq}. With this approximation, taking into account the conservation of the bulk volume, and knowing the CH_4 molality (m_{CH_4}=0.1308 molal), the liquid–gas homogenisation point is calculated at P=161 bar and T=141 °C, i.e. 4 °C below T_{trap}.

There are cases reported in the literature, where petroleum inclusions associated genetically with aqueous inclusions are characterized by very low dissolved CH_4 (see Figs. 8 and 9 of Benchilla et al., 2003), and were not understood up to now. The hypothesis proposed in this work could be a starting point to investigate. A good way to check this would be to look for correlations between CH_4 molalities and trapping temperatures, as the CH_4 solubility is temperature dependent (see right part of Fig. 2A). Paradoxically, this would justify a posteriori the use of the method of crossing isochors in some cases. However this model does not seem to be systematic.

Otherwise, this example confirms that the trapping pressure of coeval aqueous and petroleum inclusions cannot be estimated by assuming a H_2O–CH_4 composition only for aqueous inclusions. In this example, this error would yield a trapping pressure underestimated by a factor of 2 (152 bar instead of 329 bar).

4. Estimations of the trapping pressures of aqueous inclusions

4.1. The method

Neglecting hydrocarbon compounds like C_2H_6, C_3H_8, and compounds of higher molecular weights can lead to important underestimations of the trapping pressures of aqueous inclusions. A method is proposed here to evaluate the uncertainties about pressure estimations. The purpose is to calculate a trapping pressure of interstitial waters in equilibrium with an a priori petroleum composition. Such a problem cannot be solved by conventional flash or bubble-point calculations of liquid–gas phase equilibria (Asselineau et al., 1979; Thiéry et al., 2002). Indeed, the hydrocarbon composition of the petroleum is assumed, but its water content is ignored; and only the CH_4 molality is known for the aqueous solution. Thus, a specific algorithm has

to be implemented and is composed of the following steps:

1. Assume an initial hydrocarbon composition for the petroleum on a water-free basis.
2. By trial and error, estimate the H_2O content of the petroleum at the trapping point. This is done by calculating the $L(W)$ curve (i.e. the dew curve) of the petroleum for a given H_2O content and plotting it in a T–m_{CH_4} diagram (Fig. 4A). The calculated curve runs either above (or below) the ($T_h^{aq.}$–m_{CH_4}) point of the fluid inclusion. In this case, decrease (or increase) in the H_2O content. The best-fitting value is found when the $L(W)$ curve goes perfectly through the ($T_h^{aq.}$–m_{CH_4}) point of the fluid inclusion.
3. Then, read the P_{trap} pressure along the $L(W)$ curve (Fig. 4B) at $T=T_{trap}$. As the homogenisation temperature may be slightly smaller than the trapping temperature, it is proposed to add 1 to 4 °C to $T_h^{aq.}$ to

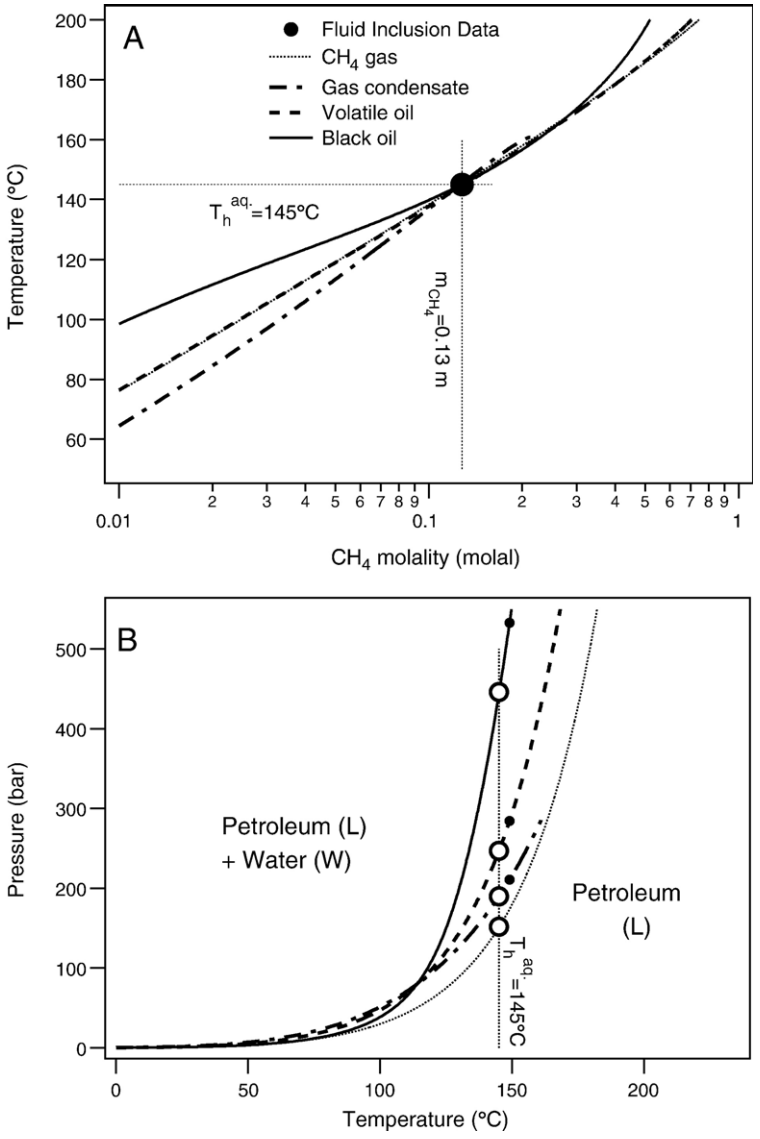

Fig. 4. Thermodynamic modelling of aqueous CH_4-bearing fluid inclusions ($T_h^{aq.}=145$ °C and $m_{CH_4}=0.13$) by considering equilibrium with one of four possible hydrocarbon-rich fluids (CH_4 fluid: dotted line; gas condensate: dashed and dotted line; volatile oil: dashed line; black oil: solid line). (A) Calculated $L(W)$ curves in a T–m_{CH_4} diagram. For a given hydrocarbon composition, the predicted $L(W)$ curve must run through the ($T_h^{aq.}$–m_{CH_4}) point of the aqueous fluid inclusion (filled circle). (B) Calculated $L(W)$ curves in the P–T diagram. Trapping pressures are obtained from $L(W)$ curves. Empty circles indicate trapping pressures by assuming $T_h^{aq.}=T_{trap}$. Filled circles yield trapping pressures by taking into account the small gap between $T_h^{aq.}$ and T_{trap}.

obtain T_{trap}. No temperature correction is required for a CH_4 gas.

This procedure can be repeated on several petroleum types to get an estimation interval of trapping pressures. The first step is the most delicate, as there is no definite and precise way for selecting the adequate petroleum composition. If traces of paleo-petroleums have been conserved in petroleum fluid inclusions, methods, based on microthermometry and volumetry, can be used (Aplin et al., 1999; Thiéry et al., 2002). However, these techniques cannot estimate unambiguously the CH_4 mole fraction of the petroleum, which is the most important parameter. Fortunately, the nature and amount of heavy hydrocarbons have less influence, and some incertitude on these data is allowed. If the type of paleo-petroleum is known, Table 2, which gives some reasonable ranges of the CH_4 mole fractions, can be used.

4.2. Application

The application of the method is illustrated on an example of aqueous inclusions, homogenising at $T_h^{aq.}=145$ °C and with a measured $m_{CH_4}=0.13$ by Raman spectroscopy. Four types of hydrocarbon-rich fluids (pure CH_4 gas, gas condensate, volatile oil and black oil), whose theoretical compositions are given in Table 3, have been used. For each fluid category, the H_2O content and the trapping pressure have been determined, as explained above. Results are given in Fig. 4 and in Table 4. In Fig. 4A are drawn the best-fitted $L(W)$ curves for each fluid type, which run through the ($T_h^{aq.}$–m_{CH_4}) point of the aqueous fluid inclusion. This gives also the H_2O content of the hydrocarbon-rich fluid (Table 4). Then, from each calculated $L(W)$ curve, the trapping pressure at $T=T_h^{aq.}$ (Fig. 4B and Table 4) is obtained. Results of this simulation reveal that the trapping pressure depends strongly from the fluid type. Pressures are the lowest (152 bar) for pure CH_4 gas and the highest for heavy oils (up to 550 bar). As the slopes of $L(W)$ curves get steeper with increasing amount of heavy hydrocarbons in petroleums, this increases considerably the uncertainties on trapping pressures. Fig. 4B shows clearly that the trapping pressure cannot be estimated reliably from Raman data of m_{CH_4} alone if interstitial waters are equilibrated with a volatile or black oil.

Another serious limitation of this method as a tool to reconstitute trapping pressures is that the Daridon equation of state (Daridon, 1992; Daridon et al., 1993) does not take into account salts. Other thermodynamic models (Søreide and Whitson, 1992; Pedersen et al., 2001; Sørensen et al., 2002) exist for H_2O–hydrocarbons–salts systems and could address this problem. But it is not the key point of this work, as hydrocarbons influence certainly aqueous salts-bearing inclusions in the same way than salts-free inclusions. The main conclusions of this work should probably be not modified in a salt-bearing system.

Table 2
Ranges of CH_4 mole fractions for typical petroleums and gases

Petroleum type	CH_4, mol %
Dry gas	95
Wet gas	90
Gas condensate	70–80
Volatile light oil	50–60
Heavy black oil	25–30

Table 3
Composition of theoretical petroleums or gas

Component, mol %	Gas condensate	Volatile oil	Black oil
CH_4	78.4	59.5	30.7
C_2H_6	8.1	14.6	12.5
C_3H_8	4.4	4.9	10.2
i-C_4H_{10}	1.2	1.9	0.6
n-C_4H_{10}	1.9	2.5	7.1
i-C_5H_{12}	1.2	1.0	1.4
n-C_5H_{12}	0.8	1.1	4.4
n-C_6H_{14}	1.5	1.6	2.5
n-C_7H_{16}	0.9	3.1	4.8
n-C_8H_{18}	0.7	1.9	4.3
n-C_9H_{20}	0.5	2.1	4.3
n-$C_{10}H_{14}$	0.3	1.3	6,4
n-$C_{12}H_{26}$	0.1	1.4	5,1
n-$C_{16}H_{34}$	0.0	1.9	5.7
Total	100	100	100

5. Conclusion

Aqueous inclusions formed in petroleum environments are traditionally treated in the H_2O–CH_4–salts system. This is justified by the fact that hydrocarbons (C_2H_6, C_3H_8, and other compounds of higher molecular weight) are in general not detectable because of their low solubility in water. This work shows that the interpretation of the microthermometric and spectrometric data of such fluid inclusions may not be not as simple as it may be thought. The P–T–X trapping conditions may modify drastically the properties of aqueous fluid inclusions, in particular the amount of dissolved methane in the aqueous part. A correct interpretation requires to take into account the system in its whole, and in particular, the hydrocarbon-rich phase that was

Table 4
Thermodynamic modelling of aqueous CH_4-bearing fluid inclusions (T_h^{aq}=145 °C and m_{CH_4}=0.13 molal) by considering four possible hydrocarbon-rich fluids (CH_4 gas, gas condensate, volatile oil, black oil)

Fluid type	H_2O, mol %	$P_h^{aq.}$, bar	T_{trap}, °C	P_{trap}, bar	m_{CH_4}, molal	$m_{C_2H_6}$, molal	$m_{C_3H_8}$, molal
CH_4 gas	3.5	152	149	152	0.13	0	0
Gas condensate	1.6	190	149	211	0.13	0.013	0.005
Volatile oil	2.2	247	149	284	0.13	0.025	0.01
Black oil	3.6	446	149	532	0.13	0.041	0.02

P_{trap}: entrapment pressure. H_2O%: H_2O content of the equilibrated hydrocarbon-rich phase. m_{CH_4}: CH_4 molality (molal) of the aqueous fluid inclusion at T_{trap}. $m_{C_2H_6}$: C_2H_6 molality at T_{trap}. $m_{C_3H_8}$: C_3H_8 molality at T_{trap}.

in equilibrium with interstitial waters. This has strong implications on methods using CH_4 solubility in water, as measured by Raman microspectroscopy, to estimate the trapping pressure of aqueous inclusions (Dubessy et al., 2001; Guillaume et al., 2003). Two cases can be distinguished:

- Aqueous inclusions, which trapped interstitial waters equilibrated with a hydrocarbon-rich gas (Fig. 1 and inclusion *A* of Fig. 2), composed mainly of CH_4 and other volatile compounds. To a first approximation, trapping pressures can be determined from molality data, as long as the true gas composition (including C_2H_6 and C_3H_8) is taken into account.
- Aqueous inclusions, which trapped interstitial waters in equilibrium with a hydrocarbon-rich liquid (Fig. 3 and inclusion *B* of Fig. 2). Such inclusions contain droplets of hydrocarbon-rich phase, which may be observable or not. The methane molalities in these inclusions are not as high as expected, when they are compared to values observed in the H_2O–CH_4 system trapped at the same pressure and temperature. Trapping pressures from m_{CH_4} Raman data alone cannot be reliably estimated, as the CH_4 molalities are nearly pressure independent. Modelling shows also that the trapping temperature is slightly larger than the liquid–gas homogenisation by a few degrees (0 to 4 °C).

This work is still preliminary. Another thermodynamic model should be applied to take into account dissolved salts. Further work should be made also to describe the influence of hydrocarbons of high molecular weight on phase equilibria and the CH_4 solubility in water. Up to now, fluid inclusion studies (Dubessy et al., 2001; Guillaume et al., 2003; Tseng and Pottorf, 2002; Teinturier et al., 2002) using m_{CH_4} data obtained by Raman spectrometry never considered the possibility of an equilibrium with a hydrocarbon phase other than pure CH_4. Such a point of view should be revised in the future.

Acknowledgements

Dr. Ronald Bakker, an anonymous reviewer, and Prof. David Rickard, as editor are deeply thanked for their constructive comments. This work has benefited from financial support from INTAS workgroup "Supercritical aqueous systems: structure, phase behaviour and thermodynamics". **[DR]**

References

Aplin, A.C., Mcleod, G., Larter, S.R., Pedersen, K.S., Sorensen, H., Booth, T., 1999. Combined use of confocal laser microscopy and PVT simulation for estimating the composition and physical properties of petroleum in fluid inclusions. Mar. Pet. Geol. 16, 97–110.

Asselineau, L., Bogdanic, G., Vidal, J., 1979. A versatile algorithm for calculating vapour–liquid equilibria. Fluid Phase Equilib. 3, 273–280.

Benchilla, L., Guilhaumou, N., Mougin, P., Jaswal, T., Roure, F., 2003. Reconstruction of palaeo-burial history and pore fluid pressure in foothill areas: a sensitivity test in the Hammam Zriba (Tunisia) and Koh-i-Maran (Pakistan) ore deposits. Geofluids 3, 103–123.

Chen, H., Wang, J., Xie, Y., Wang, Z., 2003. Geothermometry and geobarometry of overpressured environments in Qiongdongnan Basin, South China Sea. Geofluids 3, 177–187.

Daridon, Jean Luc, 1992. Mesure et représentation des équilibres de phases sous pression de mélanges d'eau, de paraffines et de dioxyde de carbone. PhD Thesis. Université de Pau et des Pays del'Adour. 177 pp.

Daridon, J.L., Lagourette, H., Saint-Guirons, H., Xans, P., 1993. A cubic equation of state model for phase equilibrium calculation of alkane+carbon dioxide+water using a group contribution k_{ij}. Fluid Phase Equilib. 91, 31–54.

de Hemptinne, J.C., Peumery, R., Ruffier-Meray, V., Moracchini, G., Naiglin, J., Carpentier, B., Oudin, J.L., Connan, J., 2001. Compositional changes resulting from the water-washing of a petroleum fluid. J. Pet. Sci. Eng. 29, 39–51.

Diamond, L., 2002. Systematics of H_2O inclusions. In: Samson, A., Anderson, D. (Eds.), Fluid Inclusions: Analysis and Interpretation, Short Course Volume, vol. 32. Min. Ass., Canada. 370 pp.

Duan, Z., Moller, N., Greenberg, J., Weare, J.H., 1992. The prediction of methane solubility in natural waters to high ionic strength from 0° to 250 °C and from 0 to 1600 bars. Geochim. Cosmochim. Acta. 56, 1451–1460.

Dubessy, J., Buschaert, S., Lamb, W., Pironon, J., Thiéry, R., 2001. Methane-bearing aqueous fluid inclusions: Raman analysis, ther-

modynamic modeling and application to petroleum basins. Chem. Geol. 173, 193–205.

Dutkiewicz, A., Ridley, J., Buick, R., 2003. Oil-bearing CO_2–CH_4–H_2O fluid inclusions: oil survival since the Palaeoproterozoic after high temperature entrapment. Chem. Geol. 194, 51–79.

Goldstein, R.H., Reynolds, T.J., 1994. Systematics of fluid inclusions in diagenetic minerals. SEPM Short Course 31 (199 pp.).

Guilhaumou, N., Ellouz, N., Jaswal, T.M., Mougin, P., 2000. Genesis and evolution of hydrocarbons entrapped in the fluorite deposit of Koh-i-Maran (North Kirthar Range Pakistan). Mar. Pet. Geol. 17, 1151–1164.

Guillaume, D., Teinturier, S., Dubessy, J., Pironon, J., 2003. Calibration of methane analysis by Raman spectroscopy in H_2O–NaCl–CH_4 fluid inclusions. Chem. Geol. 194, 41–49.

Hanor, J.S., 1980. Dissolved methane in sedimentary brines: potential effect on the PVT properties of fluid inclusions. Econ. Geol. 75, 603–609.

Liu, D.H., Xiao, X.M., Mi, J.K., Li, X.Q., Shen, J.K., Song, Z.G., Peng, P.A., 2003. Determination of trapping pressure and temperature of petroleum inclusions using PVT simulation software—a case study of Lower Ordovician carbonates from the Lunnan Low Uplift, Tarim Basin. Mar. Pet. Geol. 20, 29–43.

Montel, F., 1993. Phase equilibria needs for petroleum exploration and production industry. Fluid Phase Equilib. 84, 343–367.

Nasrifar, K.h., Moshfegian, M., 2002. Liquid–liquid equilibria of water–hydrocarbon systems from cubic equations of state. Fluid Phase Equilib. 193, 261–275.

Pedersen, K.S., Milter, J., Rasmussen, C.P., 2001. Mutual solubility of water and a reservoir fluid at high temperatures and pressures. Experimental and simulated data. Fluid Phase Equilib. 189, 85–97.

Peng, D.Y., Robinson, D.B., 1976. A new two-constant equation of state. Ind. Eng. Chem. Fundam. 15, 59–64.

Pironon, J., Canals, M., Dubessy, J., Walgenwitz, F., Laplace-Builhe, C., 1998. Volumetric reconstruction of individual oil inclusion by confocal scanning laser microscopy. Eur. J. Mineral. 10, 1143–1150.

Roedder, E., 1984. Fluid inclusions. Review in Mineralogy, vol. 12. Mineralogical Society of America, Washington, DC. 644 pp.

Søreide, I., Whitson, C.H., 1992. Peng–Robinson predictions, CO_2, N_2 and H_2S with pure water and NaCl brine. Fluid Phase Equilib. 77, 217–240.

Sørensen, H., Pedersen, K.S., Christensen, P.L., 2002. Modeling of gas solubility in brines. Org. Geochem. 33, 635–642.

Teinturier, S., Pironon, J., Walgenwitz, F., 2002. Fluid inclusions and PVTX modelling: examples from the Garn Formation in well 6507/2-2, Haltenbanken, Mid-Norway. Mar. Pet. Geol. 19, 755–765.

Thiéry, R., Pironon, J., Walgenwitz, F., Montel, F., 2002. Individual characterization of petroleum fluid inclusions (composition and *P–T* trapping conditions) by microthermometry and confocal laser scanning microscopy: inferences from applied thermodynamics of oils. Mar. Pet. Geol. 19, 847–859.

Tseng, H.-Y., Pottorf, R.J., 2002. Fluid inclusion constraints on petroleum PVT and compositional history of the Greater Alwyn–South Brent petroleum system, northern North sea. Mar. Pet. Geol. 19, 797–809.